

Nanocrystal Energetics via Quantum Similarity Measures

M. İ. Törehan Balta and Çetin Kılıç‡

Department of Physics, Gebze Institute of Technology, Gebze, Kocaeli 41400, Turkey

E-mail: cetin_kilic@gyte.edu.tr

Abstract. We first develop a descriptor-based representation of atomic environments by devising *two* local similarity indices defined from an atom-partitioned quantum-chemical descriptor. Then we employ this representation to explore the size-, shape-, and composition-dependent nanocrystal energetics. For this purpose we utilize an *energy difference* μ that is related to the atomic chemical potential, which enables one to characterize energetic heterogeneities. Employing first-principles calculations based on the density functional theory for a set of *database* systems, viz. unary atomic clusters in the shape of regular polyhedra and the bulk solids of C, Si, Pd, and Pt, we explore the correlations between the energy difference μ and similarity indices. We find that there *exists* an interconnection between nanocrystal energetics and quantum similarity measures. Accordingly we develop a means for computing total energy differences from the similarity indices via interpolation, and utilize a *test set* comprising a variety of unary nanocrystals and binary nanoalloys/nanocompounds for validation. Our findings indicate that the similarity-based energies could be utilized in computer-aided design of nanoparticles.

‡ Author to whom any correspondence should be addressed

1. Introduction

Nanoparticles exhibit chemical and structural inhomogeneities insomuch as they appear in various morphologies, regardless of the production method used[1, 2, 3]. Even a well-crystallized nanoparticle with a well-defined polyhedral shape consists of low-coordinated surface atoms that are obviously dissimilar to high-coordinated (bulk-like) atoms. One recognizes immediately by inspection that the bulk-like atoms have indeed a local (bonding) environment that resembles the *bulk solid* whereas the surface atoms along the edges or at the corners have similarities with the atoms of *atomic clusters* in regard to bonding and local coordination. Utilizing these similarities (or dissimilarities) in elucidating the properties of nanoparticles would be rewarding since one could then employ similarity search methods[4, 5, 6] in computer-aided design of nanoparticles with customized properties. We should like to complement this consideration by noting that similarity measures/indices[7, 8, 9] based on quantum-chemical descriptors[10, 11, 12] have long been available, which proved to be promising in carrying out various tasks related to a multitude of physicochemical phenomena, such as comparing properties and reactivities of different molecular systems[13], deriving quantitative structure-activity or -property relationships[14, 15], and identification of the active molecular sites[16]. Clearly these efforts demonstrate the utility of the similarity-based analysis in molecular design[17]. On the other hand, the structure and/or properties of nanoparticles have *never* been explored via the notion of the (quantum) similarity. This is, in our opinion, due to lacking a *complete*[18] similarity-based representation of atomic environments, which furnishes an adequate description for the nanoparticle atoms. The present study is thus devoted to fulfill an objective along this line: First, we develop a descriptor-based representation of atomic environments by devising *two* local similarity indices that are defined from the atom-partitioned[19, 20] *shape function*[21, 22, 23] $\sigma(\mathbf{r}) = \rho(\mathbf{r})/N_e$, where $\rho(\mathbf{r})$ and N_e denote the electronic density function and number of electrons, respectively. Then, we employ this representation to explore the size-, shape-, and composition-dependent nanocrystal energetics via the notion of quantum similarity. We focus on an *energy difference* μ , which is related to the *atomic chemical potential*, for its utility in the modelling and simulation of nanoparticles[24, 25]. This energy difference and the local similarity indices were obtained by performing first-principles calculations based on the density functional theory (DFT) for (i) a set of *database* systems including unary atomic clusters in the shape of regular polyhedra and the bulk solids of C, Si, Pd, and Pt, and (ii) a *test set* for validation, which includes a variety of unary nanocrystals as well as binary Pt-Pt nanoalloys and Pt-C nanocompounds. Regarding the energy difference μ as a “property” and exploring its correlations with the local similarity indices, we find that there *exists* an interconnection between nanocrystal energetics and quantum similarity measures. Furthermore, we introduce an interpolation procedure in order to obtain total energies and energy differences from the two similarity indices. The latter enables us to demonstrate that the similarity-based energies could be utilized in computer-aided design of nanoparticles.

Although one of the similarity indices (denoted by $Z_{i\alpha}$ below) employed in this study is of the same form as the local Carbó index[7, 8, 12], we find it necessary to introduce a *second* similarity index (denoted by $S_{i\alpha}$ below) in order to achieve an adequate chemical representation. Our findings reveal that using a single similarity index, cf. $Z_{i\alpha}$, leads to a bijection between $Z_{i\alpha}$ and μ *if and only if* the set of systems are restricted to include *equilibrium* structures. This has the obvious drawback that it requires *a priori* knowledge of the *equilibrium* geometries. Thus we find the introduction of a second similarity index necessary, which enables us to extend the aforementioned bijection to cover a generalized set of systems, including strained (compressed or dilated) systems. Hence the foregoing drawback is overcome by using *two* similarity indices with adequately tailored functional forms given below. It should be emphasized that this approach makes a similarity-based representation of the potential energy surfaces[26] accessible thanks to the inclusion of the strained systems, which facilitates an adequate description of physicochemical processes.

The rest of the paper is organized as follows: The next section is devoted to the methodological aspects which also summarizes the computational details. This is followed by a discussion of the calculation results before concluding remarks given in the last section.

2. Methodology

In this section we first define the energy difference μ and the similarity indices that constitute the employed chemical representation. We then describe (i) the set of *database* systems that are used to construct a database for the purpose of exploring correlations between energy differences and local similarity indices, and (ii) the *test set* employed for validation. Next we introduce an *ad hoc* interpolation procedure that enables one to compute the similarity-based energy differences and total energies. We finalize this section with a description of our computational modelling framework.

2.1. Energy differences

The aforementioned energy difference is defined by

$$\mu(N, d) = \Delta H_a + [E_N(d) - E_b(d_b)], \quad (1)$$

where N is the number of atoms in the system under consideration, $E_N(d)$ is the DFT-calculated energy per atom for the system with the nearest-neighbor distance d , $E_b(d_b)$ is the DFT-calculated energy per atom for the bulk solid with the *equilibrium* nearest-neighbor distance d_b corresponding to the minimum of the total energy, and ΔH_a denotes the negative of the measured[27] *heat of atomization* for the bulk solid. It is useful to define $\mu_e(N) = \mu(N, d_e)$ for the *equilibrium* value d_e of the nearest-neighbor distance. Note that $\mu_e(N)$ would be equal to the *atomic* chemical potential at zero temperature ($T = 0$ K) for a *unary* system if the *zero of energy* is set to the energy of the atom, i.e., $\mu_{\text{atom}} = 0$. Recent investigations[24, 25] by one of the present authors have indicated

that the energy difference μ could be utilized to introduce a *scale* of energy on which small (less stable, more reactive) and large (more stable, less reactive) nanocrystals are naturally ordered near the higher (μ_{atom}) and lower (μ_{bulk}) ends of the scale, respectively.

2.2. Local similarity indices

In the present study, the isolated (free) atom is employed as a *reference* system for each atomic species: namely, the free C, Si, Pd, or Pt atoms are used as a reference for the C, Si, Pd, or Pt atoms in any system, viz. atomic clusters, bulk solids, or nanocrystals, respectively. This is advantageous for computational efficiency and avoids the need for an alignment[28, 29, 30] procedure. It implies that the similarity of an atom of a certain type in a system is measured with respect to the free atom of the same type, regardless of the type of the system (atomic cluster, bulk solid, or nanocrystal). The local (atom-partitioned) Carbó index, which here serves as an indicator of similarity of an atom i , located at \mathbf{R}_i , of type α in the system under consideration to the free α atom, could then be expressed as

$$Z_{i\alpha} = \frac{\int \sigma(\mathbf{r})w_i(\mathbf{r} - \mathbf{R}_i)\sigma_\alpha(\mathbf{r})d\mathbf{r}}{\sqrt{\int \sigma^2(\mathbf{r})w_i(\mathbf{r} - \mathbf{R}_i)d\mathbf{r}}\sqrt{\int \sigma_\alpha^2(\mathbf{r})d\mathbf{r}}}, \quad (2)$$

where $\sigma(\mathbf{r})$ and $\sigma_\alpha(\mathbf{r})$ denote the shape function of the system under consideration and free α atom, respectively. The use of the Hirschfeld partitioning[19, 20] function $w_\alpha(\mathbf{r} - \mathbf{R}_\alpha) = \rho_\alpha(\mathbf{r} - \mathbf{R}_\alpha)/\rho_m(\mathbf{r})$ in equation (2) is encouraged[12] by the holographic electron density theorem[8]. Here $\rho_\alpha(\mathbf{r} - \mathbf{R}_\alpha)$ denotes the electron density of the isolated atom α located at point \mathbf{R}_α , and $\rho_m(\mathbf{r}) = \sum_\alpha \rho_\alpha(\mathbf{r} - \mathbf{R}_\alpha)$ is the promolecular electron density. As explained above, using $Z_{i\alpha}$ does not suffice for obtaining a full-fledged representation of atomic environments. Thus we introduce a *second* indicator of local similarity given by

$$S_{i\alpha} = \frac{\int r^2\sigma(\mathbf{r})w_i(\mathbf{r} - \mathbf{R}_i)\sigma_\alpha(\mathbf{r})d\mathbf{r}}{\sqrt{\int r^2\sigma^2(\mathbf{r})w_i(\mathbf{r} - \mathbf{R}_i)d\mathbf{r}}\sqrt{\int r^2\sigma_\alpha^2(\mathbf{r})d\mathbf{r}}}. \quad (3)$$

As explained below, the introduction of $S_{i\alpha}$ enables one to treat *energetic trends* when the variations with the interatomic distance d are taken into account. Note that $S_{i\alpha} = Z_{i\alpha} = 1$ if the system itself is the free α atom.

2.3. The set of database systems

In this study, first-principles calculations are employed for building a database that comprises μ and $(Z_{i\alpha}, S_{i\alpha})$ values for the *unary* atomic clusters in the shape of Platonic or Archimedean solids. In addition to these regular polyhedra, dimers C_2 , Si_2 , Pd_2 , and Pt_2 , and the bulk solids of C, Si, Pd, and Pt are included in this database. It should be emphasized that not only equilibrium systems ($d = d_e$) but also *compressed* or *dilated* systems ($d < d_e$ or $d > d_e$) are included in this set. The systems in this set are called here *database* systems for ease of speech, which are thoroughly used for the purpose of exploring the correlations between the μ and $Z_{i\alpha}$ or $S_{i\alpha}$ values. That

the set of *database* systems comprise only *equivalent* atoms makes it possible to set $E_N = E_{\text{DFT}}/N$ in equation (1), where E_{DFT} denotes the DFT-calculated total energy. For each *database* system, plotting μ values as a function of $Z_{i\alpha}$ yields a convex curve that could accurately be parameterized, as demonstrated below. Accordingly, for a given *database* system i , the energy difference defined in equation (1) is represented by $\mu = \mu_i(Z_{i\alpha})$ where μ_i denotes a polynomial function of fourth order (whose coefficients are determined by fitting to the DFT-calculated values). It is found that one must employ a distinct function μ_i with a unique set of polynomial coefficients for each system. Thus the $\mu = \mu_i(Z_{i\alpha})$ relationships are tabulated for all *database* systems with $\alpha = \text{C, Si, Pd, Pt}$ in tables 1-4 in Supplementary Data.

2.4. Test set

As mentioned above, a variety of nanocrystals are utilized as *test* systems for the purpose of validation, which exhibit structural inhomogeneity owing to the presence of a number of *inequivalent* atoms. This *test* set is designed to cover a variety of nanocrystal sizes and shapes as well as a range of nanoalloy compositions with various mixing patterns. Thus a number of unary C, Si, Pd, or Pt nanocrystals (Supplementary Data, table 5), uniformly mixed (Supplementary Data, table 6), core-shell segregated (Supplementary Data, table 7), and phase separated (Supplementary Data, table 8) Pt-Pd nanoalloys, and Pt-C nanocompounds (Supplementary Data, table 9) are contained in the *test* set. In practice, the atoms of the *test* systems were constrained to occupy the diamond (C and Si nanocrystals), fcc (Pd and Pt nanocrystals and Pt-Pd nanoalloys), and zinc-blende (Pt-C nanocompounds) lattice sites. It should be mentioned that platinum carbide nanocrystals are considered here only for the purpose of studying some challenging systems since the bonding characteristics of platinum carbide, which was synthesized[31] for the first time in 2005 under extreme conditions via a high-pressure and high-temperature method in a diamond anvil cell with laser heating, is peculiar owing to the mixed covalent-ionic-metallic[32] interatomic interactions.

2.5. Interpolation procedure

With the aid of tabulated $\mu = \mu_i(Z_{i\alpha})$ relationships (Supplementary Data, tables 1-4), the energies of the *test* systems are obtained according to the following procedure: The contribution δE_I to the energy by the I atom of a *test* system is obtained, via interpolation, by

$$\delta E_I = \sum_i \omega_{Ii} \mu_i(Z_{i\alpha}), \quad (4)$$

$$\omega_{Ii} = \frac{(S_{I\alpha} - S_{i\alpha})^{-2}}{\sum_i (S_{I\alpha} - S_{i\alpha})^{-2}}, \quad (5)$$

where ω_{Ii} denotes the interpolation coefficients, and i is the label for *database* systems (whereas I denotes atoms of the *test* system under consideration). Performing a sum

over I yields a similarity-based *total* energy difference

$$\Delta E_{\text{sim}} = \sum_I \delta E_I. \quad (6)$$

Note that ΔE_{sim} should be compared to a DFT-calculated *total* energy difference given by

$$\Delta E_{\text{DFT}} = m\Delta H_a^A + n\Delta H_a^B + [E_{\text{DFT}}(A_m B_n) - mE_b^A - nE_b^B], \quad (7)$$

for a nanoalloy/nanocompound made of m A and n B atoms, owing to the inclusion of ΔH_a and E_b in the definition of μ , cf. equation (1). One obviously needs to set $n = 0$ in equation (7) for a unary nanocrystal made of m A atoms.

2.6. Computational details

The DFT-calculated energies employed in equations (1) and (7) as well as shape functions employed in equations (2) and (3) were obtained within the generalized gradient approximation (GGA) using the PBE exchange correlation potential[33], and employing the projector augmented-wave (PAW) method[34], as implemented in VASP code[35, 36, 37]. Spin-polarization was taken into account and *scalar* relativistic effects were included in all calculations. The $2s$ and $2p$, $3s$ and $3p$, $4d$ and $5s$, and $5d$ and $6s$ states are treated as valence states for carbon, silicon, palladium, and platinum, respectively. Plane wave basis sets were used to represent the electronic states, which were determined by imposing a kinetic energy cutoff of 400, 245, 250, and 230 eV for C, Si, Pd, and Pt, respectively. Primitive and/or conventional unit cells were used in the calculations for the bulk solids, viz. C and Si in the diamond structure and Pd and Pt in the face-centered-cubic (fcc) structure, whose Brillouin zones were sampled by fine \mathbf{k} -point meshes generated according to Monkhorst-Pack scheme[38], ensuring convergence with respect to the number of \mathbf{k} -points. A variety of cubic supercells with a side length in the range 15–30 Å were used for the atomic clusters and nanocrystals, which included a vacuum region that put at least 10 Å distance between nearest atoms of two systems in neighboring supercells. Only Γ -point was used for Brillouin zone sampling in the case of the cluster or nanocrystal supercells. The error bar for the energy convergence was on the order of 1 meV/atom in all calculations.

The overlap integrals employed in equations (2) and (3) were evaluated via an adaptive multidimensional integration routine[39] within a spherical region about the atomic centers in real space. For efficiency in computing the integrands in equations (2) and (3), spline interpolations[40] of the electron density functions $\rho(\mathbf{r})$ and $\rho_\alpha(\mathbf{r})$ were performed using the three-dimensional gridded data written by VASP. The integration region for any atom α was imposed by setting the integrands to zero at every point \mathbf{r} where $\rho_\alpha(\mathbf{r}) < 3 \times 10^{-6} \text{ e}/\text{Å}^3$. That this approach yields sufficiently accurate results was checked by computing the normalization integrals such as $\int \sigma(\mathbf{r}) d\mathbf{r} = 1$ and also the integrals such as $\int \sigma(\mathbf{r}) w_i(\mathbf{r} - \mathbf{R}_i) d\mathbf{r}$ which should yield $1/N$ for the atomic clusters in the shape of Platonic or Archimedean solids. For infinite systems such as bulk solids (for which the shape function is zero everywhere but normalized to unity[22]) one could still

apply this approach thanks to the inclusion of the denominator terms in equations (2) and (3), and *spatial localization* imposed by the partitioning function $w_i(\mathbf{r} - \mathbf{R}_i)$. It was, however, required to use a sufficiently large supercell in which the region of integration is well confined. Furthermore, it was found that the integrals of the types $\int \sigma(\mathbf{r})w_i(\mathbf{r} - \mathbf{R}_i)\sigma_\alpha(\mathbf{r})d\mathbf{r}$ and $\int \sigma^2(\mathbf{r})w_i(\mathbf{r} - \mathbf{R}_i)d\mathbf{r}$ show slow convergence with respect to the supercell size whereas the ratio $\int \sigma(\mathbf{r})w_i(\mathbf{r} - \mathbf{R}_i)\sigma_\alpha(\mathbf{r})d\mathbf{r} / \sqrt{\int \sigma^2(\mathbf{r})w_i(\mathbf{r} - \mathbf{R}_i)d\mathbf{r}}$ converges rather quickly. Hence sufficiently large supercells were used in the computation of $Z_{i\alpha}$ and $S_{i\alpha}$ for the bulk solids, and it was confirmed that the computed values of $Z_{i\alpha}$ and $S_{i\alpha}$ are independent of the size of the employed supercells.

3. Results and Discussion

In this section we first investigate the correlations between the energy difference μ and local (atom-partitioned) Carbó index. We then explore the aforementioned interconnection between energetics and quantum similarity indices. Next we employ the interpolation procedure developed in the preceding section in order to devise a means for characterizing energetic heterogeneity of nanoparticles. Finally we expound the similarity-based approach developed here by comparing the similarity-based energies to DFT-calculated energies for a number of unary C, Si, Pd, or Pt nanocrystals, uniformly mixed, core-shell segregated, and phase separated Pt-Pd nanoalloys, and Pt-C nanocompounds, cf. the *test set*.

3.1. Correlations between energy differences and similarity indices

The plot of the *equilibrium* energy difference μ_e versus the local Carbó index $Z_{i\alpha}$ is displayed in figure 1(a). It is noticeable that there exists a correlation between μ_e and $Z_{i\alpha}$, which appears to be a distinct relationship for each atomic species. Note that the correlation is seemingly *linear* for the Pd and Pt systems (as marked by the dashed line passing through the set of Pt systems). Furthermore, it is seen that the set of Pd and Pt systems are grouped, i.e., they fall nearly on the same line. For the Si systems the correlation could also be regarded *approximately* linear whereas the points for the C systems fall on a monotonic curve that is *not* linear and show a more pronounced scatter. Yet, overall, there seems to exist a roughly one-to-one correspondence, i.e., bijection, between the *equilibrium* energy difference μ_e and $Z_{i\alpha}$, regardless of the atomic species. This implies that the variety of local environments sampled by the *database* systems are adequately reflected by the atom-partitioned Carbó index. On one hand, this finding implying that a single number, viz. $Z_{i\alpha}$, per atom (as opposed to a function of space) suffices to capture *energetics trends* is striking in the view of the holographic electron density theorem[8] which applies to the local electronic ground state density, i.e., a function of space restricted to some region (as opposed to a number). It could, on the other hand, be expounded by noting that *similar* atoms (viz. atoms with close $Z_{i\alpha}$ values) would exhibit *similar* energetic stability (as indicated by close μ values).

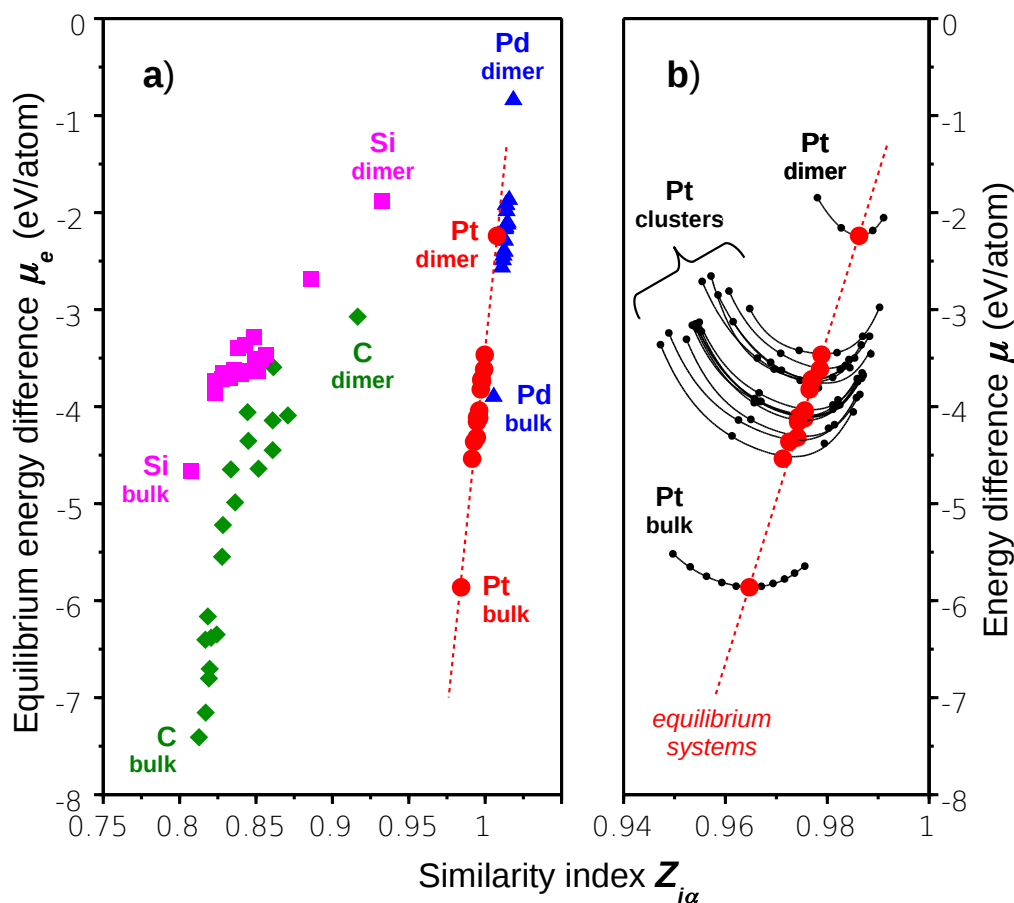


Figure 1. The equilibrium energy difference μ_e (a) and energy difference μ (b) versus the atom-partitioned Carbó index $Z_{i\alpha}$ for the unary database systems. The systems made of C, Si, Pd, and Pt atoms are represented by diamonds, squares, triangles, and circles, respectively. The points (a) or curves (b) corresponding to dimers and bulk solids are labeled while the unlabeled symbols represent the atomic clusters in the shape of regular polyhedra.

3.2. Energetics-similarity interconnection

It is obviously interesting to see if the preceding analysis for the unstrained systems could as well be applied to the (negatively or positively) strained systems, i.e., if one could introduce a generalized μ - Z relationship. Thus the plot of the energy difference μ versus the atom-partitioned Carbó index $Z_{i\alpha}$ is drawn in figure 1(b) for the Pt systems, where the small (large) circles represents strained (equilibrium) systems. Note that the large solid (red) circles as well as the (red) dashed lines on both panels of figure 1 are identical. The small (black) circles represent the DFT-calculated $(\mu, Z_{i\alpha})$ values. It is seen that the $(\mu, Z_{i\alpha})$ points fall on a distinct convex curve (represented by solid lines) for each system. This observation is of practical significance, which makes it possible to parameterize μ as a function of $Z_{i\alpha}$. In practice, this parameterization was carried out by using a distinct polynomial function $\mu_i(Z_{i\alpha}) = C_0 + C_1 Z_{i\alpha} + C_2 Z_{i\alpha}^2 + C_3 Z_{i\alpha}^3 + C_4 Z_{i\alpha}^4$ with

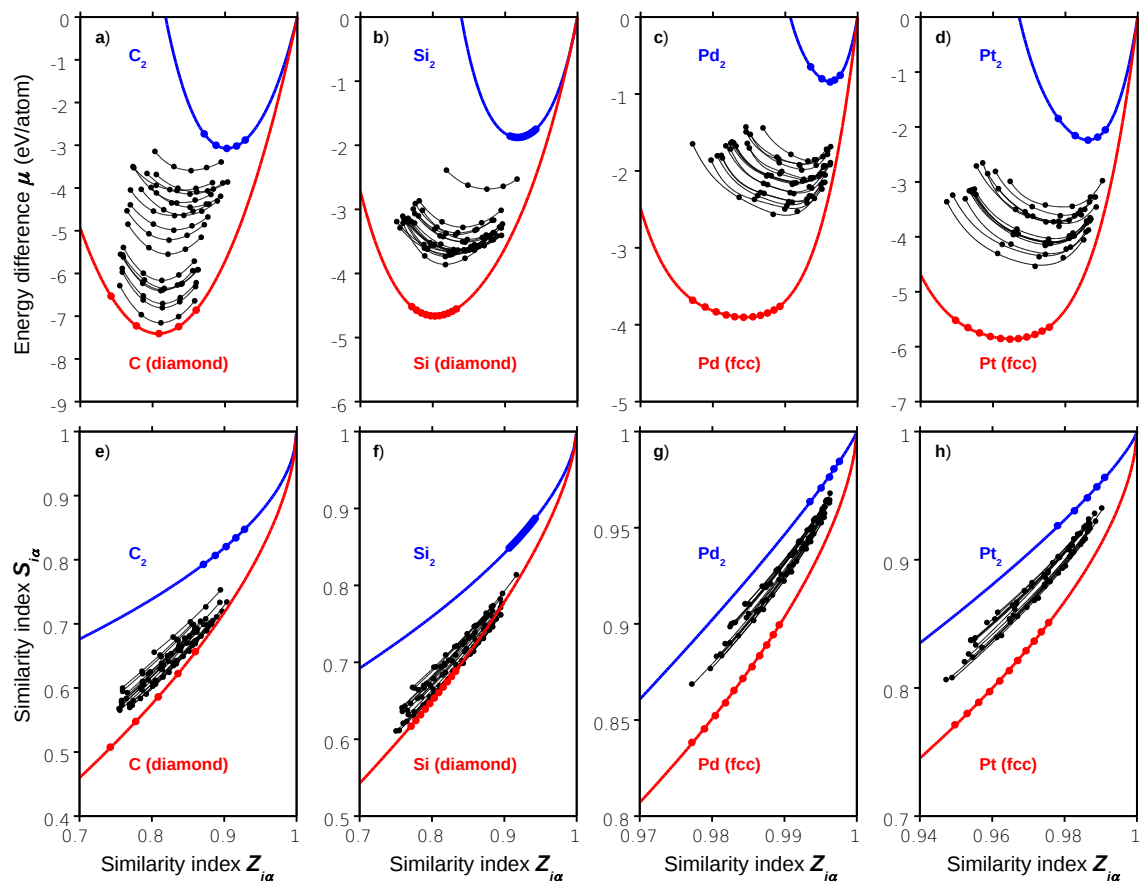


Figure 2. The energy difference μ (a)-(d) and the similarity index $S_{i\alpha}$ (e)-(h) versus the similarity index $Z_{i\alpha}$ for the C (a) and (e), Si (b) and (f), Pd (c) and (g), and Pt (d) and (h) systems. The circles represent the calculation results to which the solid-line curves are fitted. The curves corresponding to dimers and bulk solids are labeled while the unlabeled symbols represent the atomic clusters in the shape of regular polyhedra.

a unique set of polynomial coefficients $\{C_k; k = 0, 1, 2, 3, 4\}$ for each system i , yielding the solid-line curves given in figure 1(b), which are obtained via fitting to the DFT-calculated points. Repeating the same procedure for the C, Si, and Pd systems results in the μ - Z curves given in the top panels of figure 2 where, for each atomic species, the curves for the atomic clusters lay necessarily between the curves for the dimer and bulk solid. On the other hand, despite the utility of the μ - Z parameterization, there exists now *no* one-to-one correspondence between the energy difference μ and the atom-partitioned Carbó index, i.e., a given value of $Z_{i\alpha}$ does not correspond to a *unique database* system. Thus one can utilize the atom-partitioned Carbó index as a measure of similarity *only* for equilibrium systems. This, however, require *a priori* knowledge of the interatomic distances $\{d_e\}$; in other words, the equilibrium geometries. As mentioned above, this limitation is lifted by devising a *second* indicator $S_{i\alpha}$ of local similarity given in equation (3). Note that one would in principle need to use the local electronic ground state density[8] rather than numeric value of an integral of it,

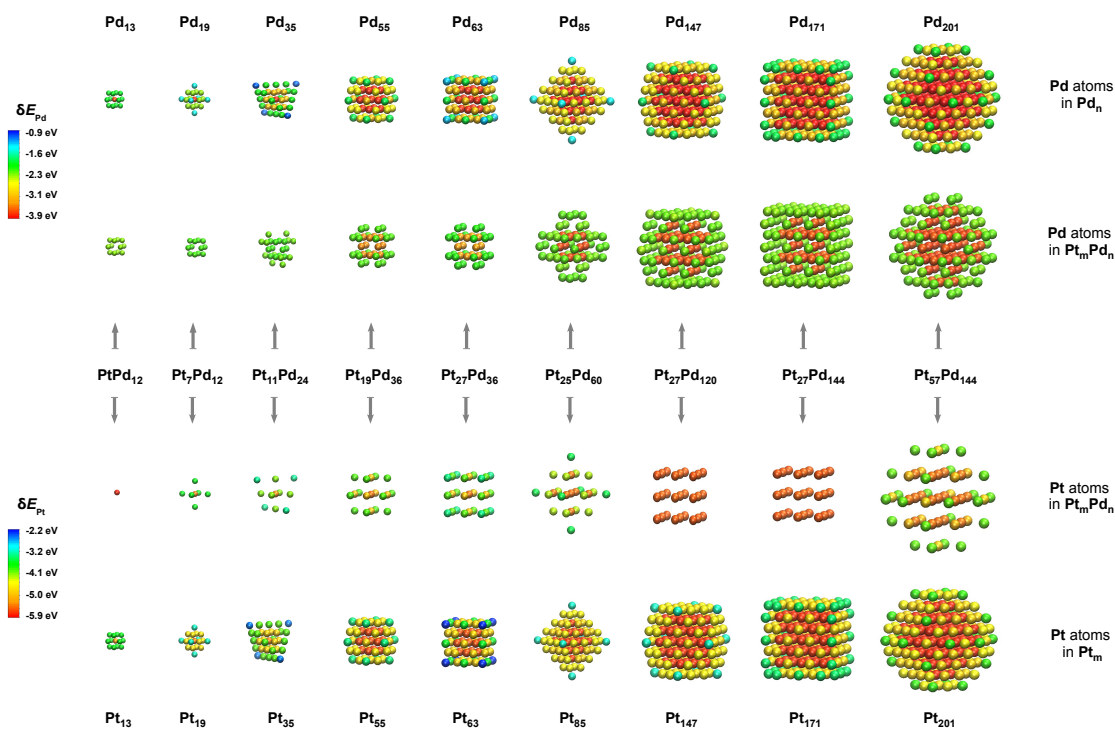


Figure 3. Color-coded graphs of δE_I computed via equation (4) for a series of Pd nanocrystals (top graphs), Pt-Pd nanoalloys (middle graphs) and Pt nanocrystals (bottom graphs). The scales on the left hand side represent the computed values of δE_I for Pd atoms (top scale) and Pt atoms (bottom scale).

viz. $Z_{i\alpha}$, in order to differentiate closely-related systems, cf. the holographic electron density theorem. Our analysis reveals that a pair of local similarity indices ($Z_{i\alpha}, S_{i\alpha}$) constitute an adequate chemical representation adopted here since a single similarity index fails to reflect *energetic trends* once the variations with the interatomic distance d are taken into account. The bottom panels of figure 2 show the plot of $S_{i\alpha}$ versus $Z_{i\alpha}$ for the *database* systems. Although the two similarity indices are not genuinely independent of each other, cf. equations (2) and (3), the $S_{i\alpha}$ - $Z_{i\alpha}$ curves appear to be distinct for each system. Furthermore all curves lie in the same region bounded by the dimer curve acting as an upper bound and the curve for the bulk solid, which serves as a lower bound. Interestingly, one could make the same observation in the top panels of figure 2, where all the μ - Z curves are also bounded by the dimer and bulk curves. Thus the S - Z curves and the μ - Z curves are roughly ordered in a similar fashion. This finding encourages one to utilize the *second* similarity index (in combination with the local Carbó index) to establish a bijection between the energy differences and similarity indices. The latter is achieved by employing the *ad hoc* interpolation formula given in equation (5), which enables one to obtain the contribution δE_I of atom I to the similarity-based total energy difference ΔE_{sim} from the similarity indices ($Z_{I\alpha}, S_{I\alpha}$).

3.3. Means for characterizing energetic inhomogeneity

Figure 3 displays color-coded graphs of δE_I values for a series of Pd nanocrystals (top graphs), Pt-Pd nanoalloys (middle graphs) and Pt nanocrystals (bottom graphs). The scales on the left hand side represent the range for the computed values of δE_I for Pd atoms (top scale) and Pt atoms (bottom scale). The higher end (blue) of these scales corresponds to less stable (more reactive) atoms while the lower end (red) corresponds to more stable (less reactive) atoms. It is encouraging to see that the bulk-like atoms near to the center of a nanocrystal have δE_{Pd} and δE_{Pt} values around the lower end whereas δE_{Pd} and δE_{Pt} values are considerably higher for the low-coordinated atoms located on the faces, along the edges, or at the corners. Thus using the δE_I values facilitates the characterization of the energetic (site-specific, morphology-dependent) inhomogeneity of the nanocrystals. Moreover *energetics trends* in regard to the size-dependence appears to be reasonable as one approach bulk-like energies in going from small to large nanocrystals. Besides using the set of δE_α or δE_β values enables one to look into local (e.g., site-specific) mixing of α - and β -type atoms in a binary alloy formation. For example, comparative inspection of Pt_{35} , $\text{Pt}_{11}\text{Pd}_{24}$, and Pd_{35} in figure 3 shows that the Pt atoms at the corners of $\text{Pt}_{11}\text{Pd}_{24}$ are less energetic in comparison those of Pt_{35} , indicating that alloying Pt nanocrystal with Pd increases the energetic stability of the corner (Pt) atoms. Since a similar analysis could be applied to any nanocrystal in a site-specific manner, using the set of δE_I values would clearly be useful in elucidating trends in the size-, shape- and composition-dependent nanocrystal energetics.

3.4. Similarity-based energies

Performing a sum over atoms as in equation (6) enables one to obtain ΔE_{sim} from the set of the atomic contributions δE_I , cf. figure 3. It is then crucial to inquire if ΔE_{sim} could be utilized in lieu of ΔE_{DFT} (calculated directly) for practical purposes, e.g., in the computer-aided design of nanocrystals. Thus the plot of ΔE_{sim} versus ΔE_{DFT} is drawn for the *test* systems in figure 4 where the calculation results are included for a variety of nanocrystal sizes and shapes as well as a range of alloy/compound compositions with various mixing patterns. Accordingly the upper, middle, and lower panels of figure 4 are devoted to the unary (C, Si, Pd, or Pt) nanocrystals, the Pt-Pd nanoalloys, the Pt-C nanocompounds, respectively. Not only unstrained but also negatively or positively strained systems are included in these panels. Here strained systems are characterized by the value of the interatomic distance d which is varied in the range of [1.37,1.55] Å for the C nanocrystals, [2.20,2.45] Å for the Si nanocrystals, [2.57,3.11] Å for the Pd nanocrystals, [2.57,2.91] Å for the Pt nanocrystals, [2.55,3.12] Å for the Pt-Pd nanoalloys, [1.90,2.25] Å for the Pt-C nanocompounds. A power-law regression analysis on the points marked by the filled symbols, which ensures that $\Delta E_{\text{sim}} \rightarrow 0$ as $\Delta E_{\text{DFT}} \rightarrow 0$, results in the dashed lines shown in the panels of figure 4, which is given by

$$\Delta E_{\text{sim}} = -C [-\Delta E_{\text{DFT}}]^\gamma \pm \delta, \quad (8)$$

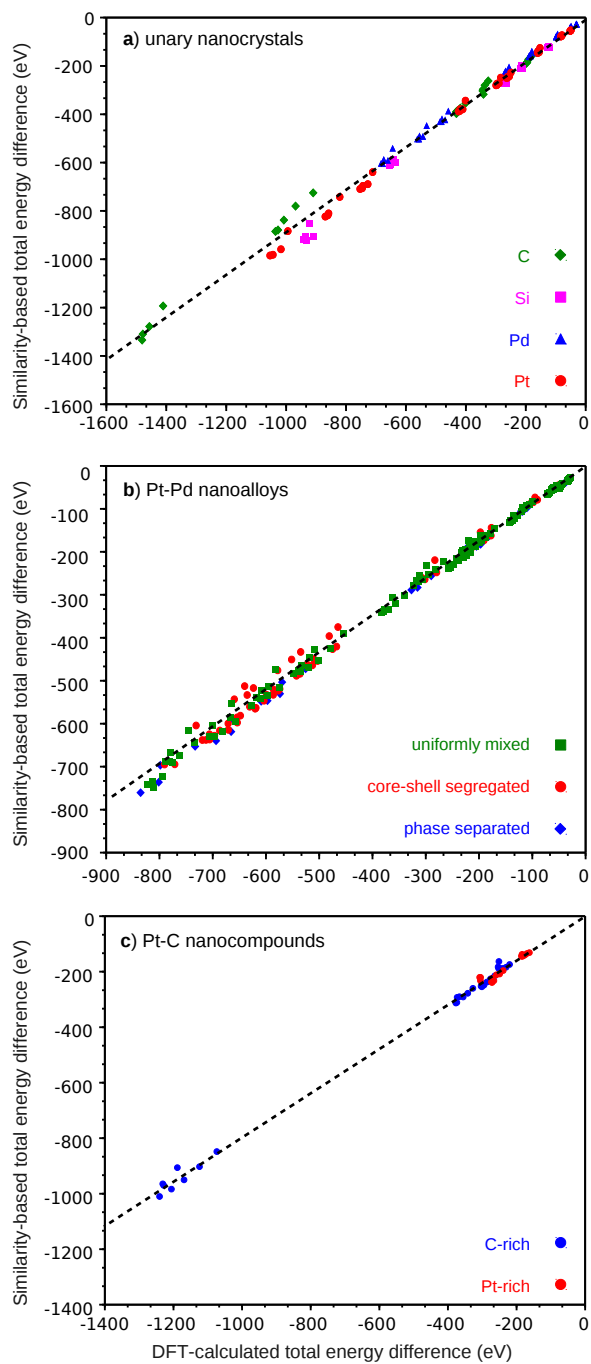


Figure 4. The similarity-based total energy difference ΔE_{sim} introduced in equation (6) versus the DFT-calculated total energy difference ΔE_{DFT} given in equation (7) for a) the unary C, Si, Pd, or Pt nanocrystals, b) the Pt-Pd nanoalloys with various mixing patterns, and c) the Pt-C nanocompounds.

Table 1. The values for the coefficient C , the exponent γ , and the error bar δ , which are introduced in equation (8), for the *test* systems.

	C	γ	δ (%)
Unary nanocrystals	1.015	0.981	5.9
Pt-Pd nanoalloys	0.929	0.989	5.9
Pt-C nanocompounds	0.775	1.005	4.3

where both ΔE_{sim} and ΔE_{DFT} are in eV, and the coefficients C , the exponents γ , and the error bars δ are listed in table 1. Note that the closeness of the values of C and γ to unity (in association with a small δ) indicates that ΔE_{sim} would follow the same *energetics trends* as ΔE_{DFT} . On the other hand, having either C or γ smaller than unity is an indication that the similarity-based interpolation procedure results in *underestimation*. The latter turns out to be the case as revealed by inspection of the slopes of the dashed lines in figure 4 as well as the entries of table 1. Yet the standard deviation δ is relatively small, i.e. on the order of 5% in all cases, i.e., not only for the unary nanocrystals but also for the Pt-Pd nanoalloys and Pt-C nanocompounds. In practice, one could invert equation (8) in order to obtain the total energy differences more accurately for these systems. It should be remarked that this description is not restricted to *equilibrium* configurations since a relatively wide range of interatomic distances are considered above. Hence, portions of the potential energy surfaces of the nanocrystals are rendered accessible. Further analysis reveals that the scatter of the points about the regression line is much less pronounced for slightly strained systems whereas significantly larger for the highly compressed systems. One should consequently recognize that the similarity-based approach exemplified here would be more suitable in describing a portion of the potential energy surface that is in the vicinity of *equilibrium*, availability of which is clearly of great service in a multitude of design problems.

It should be emphasized that ΔE_{sim} for a *test* system is *truly* obtained by use of the (quantum) similarity of its atoms to the atoms of the *database* systems. Recall that no member of the *test set* has been included in the fitting of the tabulated $\mu = \mu_i(Z_{i\alpha})$ relationships and the *database* systems are all *unary* systems. It is thus remarkable that the similarity-based description of the energetics of binary nanoalloys is almost as good as that of unary nanocrystals as seen by comparing figure 4(b) to figure 4(a). The energetics of Pt-C nanocompounds constitute a greater challenge as evidenced by the relatively large deviation of the coefficient C from unity, yet the correlation between ΔE_{sim} and ΔE_{DFT} for these systems is also significant, cf. figure 4(c), with a standard deviation $\delta < 5\%$. The latter gives evidence for the ubiquitous utility of the similarity-based approach developed here since the bonding characteristics of platinum carbide is peculiar[32] owing to the mixed covalent-ionic-metallic interatomic interactions.

4. Conclusion

The results of the present investigation show that there exists an interconnection between the energy differences utilized in the modelling and simulation of nanocrystals and the quantum similarity measures, which is established here by devising two local similarity indices given in equations (2) and (3). We show that this finding leads to the development of a new approach for computing the energy differences and total energies, which is based on the similarity of the nanocrystal atoms to the atoms of a set of *database* systems. We find that the similarity-based energy differences exhibit the same trends as those obtained directly from the DFT calculations. Subsequently, it is demonstrated that our similarity-based approach could be used to explore the size-, shape- and composition-dependent nanocrystal energetics. It should be remarked that *no* knowledge of the *equilibrium* geometries is needed *a priori* in this approach since it is sufficiently general to cover non-equilibrium configurations. In particular, it is intriguing that the similarity-based description of energetics of the binary systems is nearly as good as that of unary systems -albeit *no* binary systems are included among the *database* systems. Furthermore, it is demonstrated that our similarity-based approach provides a means for characterizing the energetic inhomogeneity of the nanocrystals, cf. figure 3. Accordingly, we project that the methodology of this paper would be of great service in informatics-driven approaches, i.e. materials informatics[41]. Besides, we anticipate that the similarity-based approach presented here could be generalized to explore other physicochemical quantities, e.g. (site-specific) adsorption energies, and could then be utilized in the surface engineering of nanocrystals.

Acknowledgments

This work was supported by TUBITAK under Grant No. TBAG-109T677. The computations were carried out at the High Performance and Grid Computing Center (TRUBA resources) of TUBITAK ULAKBIM.

References

- [1] Trindade T, O'Brien P and Pickett NL 2001 Nanocrystalline semiconductors: Synthesis, properties and perspectives *Chem. Mat.* 13 3843–3858
- [2] Ferrando R, Jellinek J and Johnston RL 2008 Nanoalloys: From theory to applications of alloy clusters and nanoparticles *Chem. Rev.* 108 845–910
- [3] Xia Y, Xiong Y, Lim B and Skrabalak SE 2009 Shape-controlled synthesis of metal nanocrystals: Simple chemistry meets complex physics? *Angew. Chem.-Int. Edit.* 48 60–103
- [4] Willett P, Barnard JM and Downs GM 1998 Chemical similarity searching *J. Chem. Inf. Comput. Sci.* 38 983–996
- [5] Sheridan RP and Kearsley SK 2002 Why do we need so many chemical similarity search methods? *Drug Discov. Today* 7 903–911
- [6] Engel T 2006 Basic overview of chemoinformatics *J. Chem. Inf. Model.* 46 2267–2277
- [7] Carbó R, Leyda L and Arnau M 1980 How similar is a molecule to another - an electron-density measure of similarity between 2 molecular-structures *Int. J. Quant. Chem.* 17 1185–1189

- [8] Mezey PG 1999 The holographic electron density theorem and quantum similarity measures *Mol. Phys.* 96 169–178
- [9] Chermette H 1999 Chemical reactivity indexes in density functional theory *J. Comput. Chem.* 20 129–154
- [10] Karelson M, Lobanov VS and Katritzky AR 1996 Quantum-chemical descriptors in QSAR/QSPR studies *Chem. Rev.* 96 1027–1043
- [11] Bultinck P and Carbó-Dorca R 2005 Molecular quantum similarity using conceptual DFT descriptors *J. Chem. Sci.* 117 425–435
- [12] Geerlings P, Boon G, Van Alsenoy C and De Proft F 2005 Density functional theory and quantum similarity *Int. J. Quant. Chem.* 101 722–732
- [13] Boon G, Langenaeker W, De Proft F, De Winter H, Tollenaere JP and Geerlings P 2001 Systematic study of the quality of various quantum similarity descriptors. Use of the autocorrelation function and principal component analysis *J. Phys. Chem. A* 105 8805–8814
- [14] Good AC, Peterson SJ and Richards WG 1993 QSARs from similarity-matrices - technique validation and application in the comparison of different similarity evaluation methods *J. Med. Chem.* 36 2929–2937
- [15] Besalú E, Girones X, Amat L and Carbó-Dorca R 2002 Molecular quantum similarity and the fundamentals of QSAR *Accounts Chem. Res.* 35 289–295
- [16] Amat L, Besalú E, Carbó-Dorca R and Ponec R 2001 Identification of active molecular sites using quantum-self-similarity measures. *J. Chem. Inform. Comput. Sci.* 41 978–991
- [17] Rouvray DH 1992 Definition and role of similarity concepts in the chemical and physical sciences *J. Chem. Inf. Comput. Sci.* 32 580–586
- [18] Bartók AP, Kondor R and Csányi G 2013 On representing chemical environments *Phys. Rev. B* 87 184115
- [19] Hirshfeld FL 1977 Bonded-atom fragments for describing molecular charge-densities *Theor. Chem. Acc.* 44 129–138
- [20] De Proft F, Vivas-Reyes R, Peeters A, Van Alsenoy C and Geerlings P 2003 Hirshfeld partitioning of the electron density: Atomic dipoles and their relation with functional group properties *J. Comput. Chem.* 24 463–469
- [21] Parr RG and Bartolotti LJ 1983 Some remarks on the density functional theory of few-electron systems *J. Phys. Chem.* 87 2810–2815
- [22] Ayers PW 2000 Density per particle as a descriptor of Coulombic systems *Proc. Natl. Acad. Sci. USA* 97 1959–1964
- [23] De Proft F, Ayers PW, Sen KD and Geerlings P 2004 On the importance of the “density per particle” (shape function) in the density functional theory *J. Chem. Phys.* 120 9969–9973
- [24] Kılıç Ç 2010 Size- and shape-dependent energetics of transition-metal nanocrystals *Solid State Commun.* 150 2333–2336
- [25] Kılıç Ç 2011 Energy-distance relation for fcc transition metal nanocrystals *EPL* 93 26004
- [26] Behler J 2011 Neural network potential-energy surfaces in chemistry: a tool for large-scale simulations *Phys. Chem. Chem. Phys.* 13 17930–17955
- [27] Lide D 2008 *CRC handbook of chemistry and physics : a ready-reference book of chemical and physical data* (Boca Raton, FL: CRC)
- [28] Parretti MF, Kroemer RT, Rothman JH and Richards WG 1997 Alignment of molecules by the monte carlo optimization of molecular similarity indices *J. Comput. Chem.* 18 1344–1353
- [29] Bultinck P, Kuppens T, Gironés X and Carbó-Dorca R 2003 Quantum similarity superposition algorithm (QSSA): A consistent scheme for molecular alignment and molecular similarity based on quantum chemistry *J. Chem. Inf. Comput. Sci.* 43 1143–1150
- [30] Bultinck P, Carbó-Dorca R and Van Alsenoy C 2003 Quality of approximate electron densities and internal consistency of molecular alignment algorithms in molecular quantum similarity *J. Chem. Inform. Comput. Sci.* 43 1208–1217
- [31] Ono S, Kikegawa T and Ohishi Y 2005 A high-pressure and high-temperature synthesis of platinum

- carbide *Solid State Commun.* 133 55–59
- [32] Ivanovskii AL 2009 Platinum group metal nitrides and carbides: synthesis, properties and simulation *Russ. Chem. Rev.* 78 303–318
- [33] Perdew JP, Burke K and Ernzerhof M 1996 Generalized gradient approximation made simple *Phys. Rev. Lett.* 77 3865–3868
- [34] Blochl PE 1994 Projector augmented-wave method *Phys. Rev. B* 50 17953–17979
- [35] Kresse G and Fürthmüller J 1996 Efficiency of ab-initio total energy calculations for metals and semiconductors using a plane-wave basis set *Comput. Mater. Sci.* 6 15–50
- [36] Kresse G and Joubert D 1999 From ultrasoft pseudopotentials to the projector augmented-wave method *Phys. Rev. B* 59 1758–1775
- [37] Sun GY, Kurtz J, Rajczyk P, Kertesz M, Hafner J and Kresse G 2003 Performance of the Vienna ab initio simulation package (VASP) in chemical applications *J. Mol. Struct. - THEOCHEM* 624 37–45
- [38] Monkhorst HJ and Pack JD 1976 Special points for brillouin-zone integrations *Phys. Rev. B* 13 5188–5192
- [39] Berntsen J, Espelid TO and Genz A 1991 Algorithm 698: Dcuhre: an adaptive multidimensional integration routine for a vector of integrals *ACM Trans. Math. Softw.* 17 452–456
- [40] Boor C 2001 *A practical guide to splines* (New York: Springer)
- [41] Rajan K 2005 Materials informatics *Mater. Today* 8 38–45

5. Supplementary Data

Table 1. The coefficients in the polynomial relationship $\mu_i(Z_{i\alpha}) = C_0 + C_1 Z_{i\alpha} + C_2 Z_{i\alpha}^2 + C_3 Z_{i\alpha}^3 + C_4 Z_{i\alpha}^4$ for the *database* systems with $\alpha = C$.

i	C_0	C_1	C_2	C_3	C_4
Dimer	-3.073	-0.020	317.605	-662.128	7537.589
Tetrahedron	-3.585	-0.243	131.127	-681.23	6174.054
Octahedron	-4.448	-0.095	142.577	-87.009	3321.910
Cube	-5.212	-0.223	166.607	-491.447	2717.141
Icosahedron	-4.089	-0.137	117.769	60.221	4425.848
Dodecahedron	-6.384	-0.008	221.448	-283.245	491.922
Cuboctahedron	-4.335	-1.519	144.830	-354.519	3219.137
Icosidodecahedron	-4.978	-0.373	145.124	-97.645	1514.808
Rhombicosidodecahedron	-4.641	-0.109	125.075	-684.302	4934.909
Rhombicuboctahedron	-4.639	-0.068	159.520	-129.355	2021.972
Snub cube	-4.140	-0.142	122.413	-7.260	3077.307
Snub dodecahedron	-4.056	-0.205	95.873	-328.335	4150.783
Truncated cube	-6.163	-0.008	245.263	-493.121	651.689
Truncated cuboctahedron	-6.704	-0.003	242.436	-347.009	452.461
Truncated dodecahedron	-6.403	-0.003	262.507	-577.442	735.888
Truncated icosahedron	-7.155	-0.001	250.095	-314.456	294.125
Truncated icosidodecahedron	-6.803	-0.001	250.759	-371.083	398.845
Truncated octahedron	-6.346	-0.146	220.742	-3.372	-833.696
Truncated tetrahedron	-5.547	-0.038	203.429	-369.196	1140.742
Bulk solid (diamond)	-7.408	-0.019	201.196	-77.268	364.538

Table 2. The coefficients in the polynomial relationship $\mu_i(Z_{i\alpha}) = C_0 + C_1Z_{i\alpha} + C_2Z_{i\alpha}^2 + C_3Z_{i\alpha}^3 + C_4Z_{i\alpha}^4$ for the *database* systems with $\alpha = \text{Si}$.

i	C_0	C_1	C_2	C_3	C_4
Dimer	-1.878	0.019	199.688	-304.137	14483.305
Tetrahedron	-2.682	-0.164	79.253	66.414	5340.125
Octahedron	-3.510	-0.127	84.063	-21.272	2699.598
Cube	-3.468	-0.114	100.733	-98.621	2757.457
Icosahedron	-3.629	-0.158	76.853	30.174	2700.339
Dodecahedron	-3.673	0.260	85.190	-350.766	3664.758
Cuboctahedron	-3.501	-0.135	84.383	-53.555	2500.681
Icosidodecahedron	-3.647	-0.075	92.153	-126.553	2048.645
Rhombicosidodecahedron	-3.622	-0.183	85.326	-77.365	1782.164
Rhombicuboctahedron	-3.636	-0.018	74.042	-10.420	2377.063
Snub cube	-3.702	-0.06	65.252	-56.723	2221.128
Snub dodecahedron	-3.650	-0.178	74.868	-52.119	1598.565
Truncated cube	-3.366	0.036	92.328	-439.824	3800.469
Truncated cuboctahedron	-3.719	0.012	118.783	-526.290	2871.248
Truncated dodecahedron	-3.396	-0.101	95.441	-254.356	2349.424
Truncated icosahedron	-3.858	-0.121	139.553	-682.515	3016.681
Truncated icosidodecahedron	-3.732	-0.133	122.766	-747.689	3783.626
Truncated octahedron	-3.654	-0.040	111.444	-98.950	1228.149
Truncated tetrahedron	-3.277	-0.104	95.328	-198.807	2581.799
Bulk solid (diamond)	-4.664	-0.005	132.739	-349.581	1444.348

Table 3. The coefficients in the polynomial relationship $\mu_i(Z_{i\alpha}) = C_0 + C_1 Z_{i\alpha} + C_2 Z_{i\alpha}^2 + C_3 Z_{i\alpha}^3 + C_4 Z_{i\alpha}^4$ for the *database* systems with $\alpha = \text{Pd}$.

i	C_0	C_1	C_2	C_3	C_4
Dimer	-0.840	-6.400	33311.393	3721206.184	511101393.400
Tetrahedron	-1.873	-2.569	16389.493	2770276.589	261971715.68
Octahedron	-2.117	-16.320	6705.320	2202612.455	273801033.220
Cube	-2.099	-16.802	9114.439	2498668.588	251443464.030
Icosahedron	-2.391	-16.539	5770.537	1412107.506	134315549.540
Dodecahedron	-2.427	-16.672	7362.723	2456123.506	341325123.540
Cuboctahedron	-2.279	-15.448	6237.267	1335147.165	149468839.650
Icosidodecahedron	-2.268	-13.721	6534.375	1066636.190	116535424.090
Rhombicosidodecahedron	-2.436	-12.002	6829.432	1021713.153	95175168.583
Rhombicuboctahedron	-2.387	-14.826	5718.681	1189598.403	121041265.850
Snub cube	-2.475	-17.289	4257.951	1043419.391	104446948.320
Snub dodecahedron	-2.569	-15.577	7444.008	890949.576	57481732.306
Truncated cube	-1.907	-13.208	5183.779	1300439.300	201545862.790
Truncated cuboctahedron	-2.143	-13.097	5912.355	1114780.637	142341680.100
Truncated dodecahedron	-1.906	-11.746	8052.126	1226154.160	163401620.030
Truncated icosahedron	-2.164	-11.775	6970.046	1165244.069	123592942.310
Truncated icosidodecahedron	-2.148	-11.657	6461.044	1068337.858	128956261.350
Truncated octahedron	-2.144	-11.828	6638.110	1336198.448	150585430.490
Truncated tetrahedron	-1.977	-11.391	8351.823	1444832.497	202017269.710
Bulk solid (fcc)	-3.901	-3.186	4385.080	265509.255	30014956.142

Table 4. The coefficients in the polynomial relationship $\mu_i(Z_{i\alpha}) = C_0 + C_1Z_{i\alpha} + C_2Z_{i\alpha}^2 + C_3Z_{i\alpha}^3 + C_4Z_{i\alpha}^4$ for the *database* systems with $\alpha = \text{Pt}$.

i	C_0	C_1	C_2	C_3	C_4
Dimer	-2.239	-1.024	6923.321	227192.717	9823552.539
Octahedron	-3.163	-1.457	2765.467	81231.426	9123526.461
Octahedron	-3.455	-1.794	1539.467	89757.477	9766553.492
Cube	-3.745	-1.180	2664.201	110609.121	9235782.643
Icosahedron	-3.965	-1.680	6354.282	98651.463	8230902.315
Dodecahedron	-3.565	-1.525	9584.201	92629.274	9256123.345
Cuboctahedron	-3.739	-10.083	1016.310	80505.616	7794825.247
Icosidodecahedron	-4.087	-5.506	1700.004	99336.991	4531031.341
Rhombicosidodecahedron	-4.301	-6.027	1741.367	85256.841	4067693.288
Rhombicuboctahedron	-4.105	-5.443	2020.654	100834.379	4306097.006
Snub cube	-4.338	-7.474	1609.428	73361.770	3170892.929
Snub dodecahedron	-4.509	-7.448	1604.538	63718.292	2772333.570
Truncated cube	-3.719	-3.514	2780.603	93706.049	3989379.764
Truncated cuboctahedron	-4.095	-5.643	2040.338	72807.266	3718101.004
Truncated dodecahedron	-3.717	-0.827	2721.354	90423.545	4418129.817
Truncated icosahedron	-4.100	-6.002	1858.331	81242.419	4454911.798
Truncated icosidodecahedron	-4.140	-5.594	2066.221	74635.086	3730411.533
Truncated octahedron	-4.027	-6.057	1886.612	98087.942	4539336.168
Truncated tetrahedron	-3.603	-6.091	2304.512	127671.403	6669393.171
Bulk solid (fcc)	-5.858	-1.159	1463.681	28636.243	1814989.886

Table 5. Unary (X=C or Si; Y=Pd or Pt) nanocrystals employed in this study.

Nanocrystal	Shape
X ₃₅	Octahedron
X ₅₁	Truncated tetrahedron
X ₅₉	Truncated tetrahedron
X ₇₅	Truncated cube
X ₁₆₅	Octahedron
X ₂₃₉	Truncated cube
Y ₁₃	Cuboctahedron
Y ₁₉	Octahedron
Y ₃₅	Tetrahedron
Y ₅₅	Cuboctahedron
Y ₆₃	Cube
Y ₈₅	Octahedron
Y ₁₄₇	Cuboctahedron
Y ₁₇₁	Cube
Y ₂₀₁	Truncated octahedron

Table 6. Uniformly mixed nanoalloys employed in this study.

	Pt Composition	Shape
Pt ₁₂ Pd	0.923	Cuboctahedron
Pt ₁₂ Pd ₇	0.632	Octahedron
Pt ₂₄ Pd ₁₁	0.686	Tetrahedron
Pt ₃₆ Pd ₁₉	0.655	Cuboctahedron
Pt ₃₆ Pd ₂₇	0.571	Cube
Pt ₆₀ Pd ₂₅	0.706	Octahedron
Pt ₁₂₀ Pd ₂₇	0.816	Cuboctahedron
Pt ₁₄₄ Pd ₂₇	0.842	Cube
PtPd ₁₂	0.077	Cuboctahedron
Pt ₇ Pd ₁₂	0.368	Octahedron
Pt ₁₁ Pd ₂₄	0.314	Tetrahedron
Pt ₁₉ Pd ₃₆	0.345	Cuboctahedron
Pt ₂₇ Pd ₃₆	0.429	Cube
Pt ₂₅ Pd ₆₀	0.294	Octahedron
Pt ₂₇ Pd ₁₂₀	0.184	Cuboctahedron
Pt ₂₇ Pd ₁₄₄	0.158	Cube
Pt ₅₇ Pd ₁₄₄	0.284	Truncated octahedron

Table 7. Core-shell segregated nanoalloys employed in this study.

	Pt Composition	Shape
PtPd ₁₈	0.053	Octahedron
PtPd ₃₄	0.029	Tetrahedron
Pt ₁₃ Pd ₄₂	0.236	Cuboctahedron
Pt ₁₃ Pd ₅₀	0.206	Cube
Pt ₁₉ Pd ₆₆	0.224	Octahedron
Pt ₁₃ Pd ₁₃₄	0.088	Cuboctahedron
Pt ₁₉ Pd ₁₂₈	0.129	Cuboctahedron
Pt ₅₅ Pd ₉₂	0.374	Cuboctahedron
Pt ₁₅₈ Pd ₁₃	0.924	Cube
Pt ₁₅₂ Pd ₁₉	0.889	Cube
Pt ₁₃₆ Pd ₃₅	0.795	Cube
Pt ₁₁₆ Pd ₅₅	0.678	Cube
Pt ₁₀₈ Pd ₆₃	0.632	Cube
Pt ₁₈₈ Pd ₁₃	0.935	Truncated octahedron
Pt ₁₈₂ Pd ₁₉	0.905	Truncated octahedron
Pt ₁₆₆ Pd ₃₅	0.826	Truncated octahedron
Pt ₁₄₆ Pd ₅₅	0.726	Truncated octahedron

Table 8. Phase separated nanoalloys employed in this study.

	Pt Composition	Shape
Pt ₄ Pd ₉	0.308	Cuboctahedron
Pt ₅ Pd ₁₄	0.263	Octahedron
Pt ₁₃ Pd ₂₂	0.371	Tetrahedron
Pt ₂₁ Pd ₃₄	0.382	Cuboctahedron
Pt ₂₅ Pd ₃₈	0.397	Cube
Pt ₃₀ Pd ₅₅	0.353	Octahedron
Pt ₆₁ Pd ₈₆	0.415	Cuboctahedron
Pt ₇₃ Pd ₉₈	0.427	Cube
Pt ₁₁₉ Pd ₈₂	0.592	Truncated octahedron

Table 9. Zincblende nanocompounds employed in this study.

	Pt Composition	Shape
Pt ₁₆ C ₁₉	0.457	Octahedron
Pt ₂₀ C ₃₁	0.392	Truncated tetrahedron
Pt ₂₈ C ₃₁	0.475	Truncated tetrahedron
Pt ₃₂ C ₄₃	0.427	Truncated cube
Pt ₈₀ C ₈₅	0.485	Octahedron
Pt ₁₀₄ C ₁₃₅	0.435	Truncated cube
Pt ₁₉ C ₁₆	0.543	Octahedron
Pt ₃₁ C ₂₀	0.608	Truncated tetrahedron
Pt ₃₁ C ₂₈	0.525	Truncated tetrahedron
Pt ₄₃ C ₃₂	0.573	Truncated cube
Pt ₈₅ C ₈₀	0.515	Octahedron
Pt ₁₃₅ C ₁₀₄	0.565	Truncated cube